

Journal of Materials Chemistry A

Accepted Manuscript



This is an *Accepted Manuscript*, which has been through the Royal Society of Chemistry peer review process and has been accepted for publication.

Accepted Manuscripts are published online shortly after acceptance, before technical editing, formatting and proof reading. Using this free service, authors can make their results available to the community, in citable form, before we publish the edited article. We will replace this *Accepted Manuscript* with the edited and formatted *Advance Article* as soon as it is available.

You can find more information about *Accepted Manuscripts* in the [Information for Authors](#).

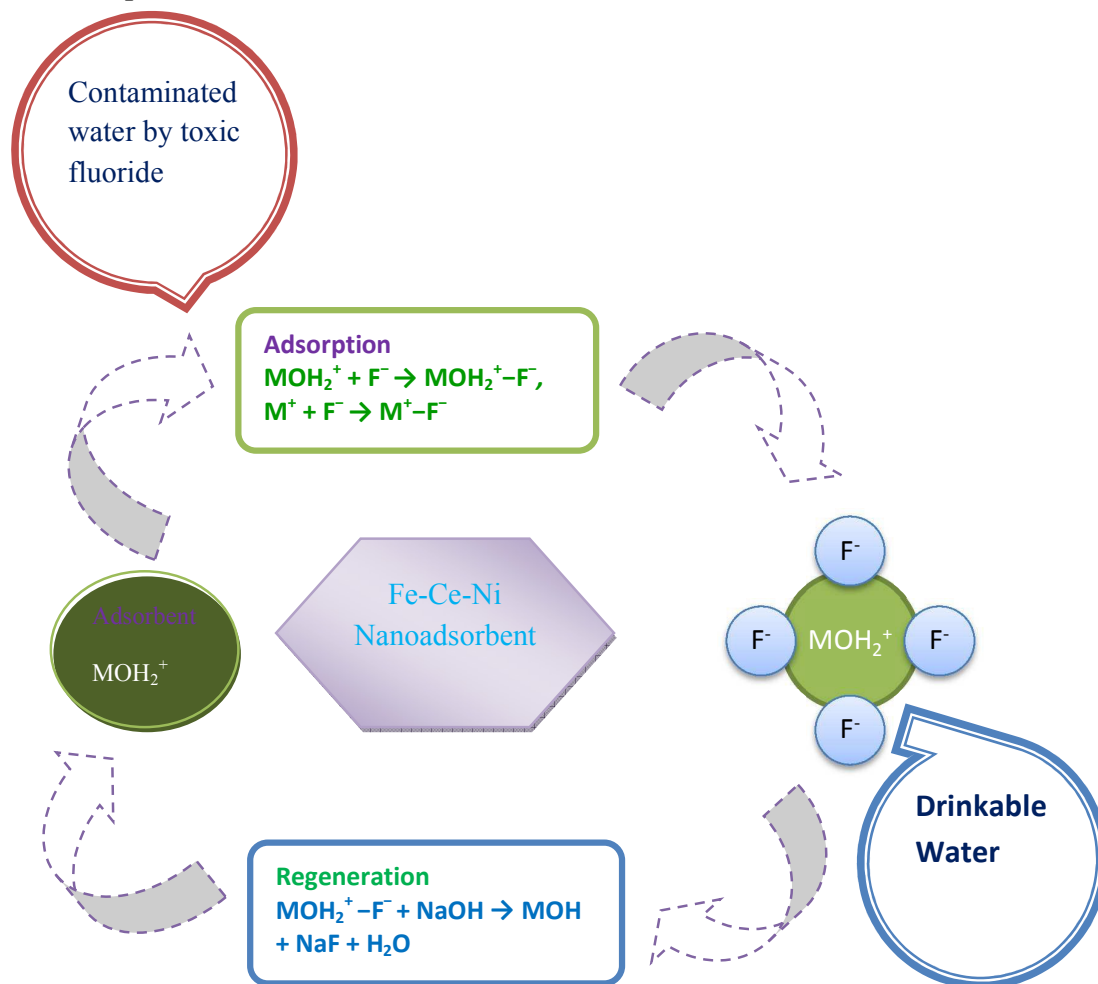
Please note that technical editing may introduce minor changes to the text and/or graphics, which may alter content. The journal's standard [Terms & Conditions](#) and the [Ethical guidelines](#) still apply. In no event shall the Royal Society of Chemistry be held responsible for any errors or omissions in this *Accepted Manuscript* or any consequences arising from the use of any information it contains.

Development of nanoporous adsorbent for the removal of health hazardous fluoride ions from aqueous systems†

Ankita Dhillon and Dinesh Kumar*

Department of Chemistry, Banasthali University, Rajasthan–304022, INDIA

Graphical Abstract



Highlight

* Corresponding author: E-mail: dsbchoudhary2002@gmail.com

†Electronic supplementary information (ESI) available: N_2 Adsorption/Desorption curves, FTIR spectra of Fe–Ce–Ni nanoadsorbent before and after fluoride adsorption, Langmuir isotherm outlines of the fluoride adsorption by nanoadsorbent, Temkin isotherm outlines of the fluoride adsorption by nanoadsorbent, Pseudo–first–order plots of the fluoride adsorption by nanoadsorbent, potentiometric titration curve of nanoadsorbent, and water quality parameters before and after treatment.

Development of a re-usable, cost-effective and sustainable nanoporous adsorbent for efficient removal of toxic fluoride ions from aqueous systems.

Abstract

A new crystalline and hybrid Fe–Ce–Ni nanoporous adsorbent was developed, and tested to establish its efficiency, kinetic and thermodynamic studies for fluoride removal. The adsorption properties of the developed adsorbent were studied using batch and column methods and the noticeable fluoride adsorption capacity was 285.7 mg g^{-1} . The pH range for maximum removal of fluoride on the metal oxide adsorbent surface was found to be 5.0–7.0. The adsorption kinetics fitted well with pseudo-second-order as compared to pseudo-first-order rate expression. Herein, four models are used to fit the experimental data to explain the adsorption isotherm. The adsorption isotherm data fitted rationally well into both Freundlich and Dubinin–Radushkevich (D–R) isotherm models. Thermodynamic examination demonstrated that fluoride adsorption on Fe–Ce–Ni nanoadsorbent was reasonably spontaneous and endothermic. Most commonly existing anions such as Cl^- , NO_3^- , SO_4^{2-} , CO_3^{2-} , HCO_3^- except PO_4^{3-} showed no significant counter ion effect on fluoride adsorption efficiency. The adsorbent was easily regenerated up to 95% with an alkali solution. The capability to revive and reuse nanoadsorbent makes it a smart sustainable material.

Introduction

Fluoride contamination in drinking water is one of the major concerns worldwide. Owing to natural and anthropogenic actions it has been proved to be hazardous not only to human health but also to the flora and fauna.¹ According to World Health Organization (WHO), in addition to arsenic and nitrate, fluoride is also one of the major chemical contaminants of water and is a source of large-scale health problems.² Various parts of the world including India are affected by the elevated fluoride concentrations in the groundwater.^{3–12} Fluoride being widely dispersed in the surroundings,¹³ is normally discharged into the surrounding groundwater by deliberate slow dissolution of fluorine-containing rocks.¹⁴ Other sources of fluoride which causes contamination of the groundwater are various minerals, like fluorite, biotites, topaz, several rocks such as granite, basalt, syenite, and shale.^{15–17} In addition to the various natural resources of fluoride enhancement in groundwater, wastes from glass and ceramic industries, electroplating, and semiconductor manufacturing factories, coal fired power stations, brick and iron works, and aluminium smelters are also a major source of

fluoride contamination.^{18,19} The effluents discharged from such industries caused ten to thousands of mg L^{-1} elevation in fluoride concentrations in natural waters.²⁰

A majority of world population has been found to depend on drinking water having fluoride concentrations higher than WHO guideline of 1.5 mg L^{-1} .²¹ Environmental Protection Agency (EPA, USA) has set enforceable and non-enforceable (secondary) drinking water standards for fluoride at 4 mg L^{-1} and 2 mg L^{-1} , respectively.²² The department of Human Health and Services (HHS) recommends Maximum Contamination Level (MCL) of fluoride as 0.7 mg L^{-1} to promote public health benefits of fluoride in potable water.²³ The European Union (EU) specifies 1.5 mg L^{-1} of fluoride in drinking water for human consumption. The impact of fluoride on the human health can be beneficial or injurious which in turn depends on the concentration and the extent of constant uptake. Particularly among children, fluoride when taken in a constricted advantageous concentration range is frequently known to comprise an advantageous effect on the speed of incidence of dental caries.²⁴ In contrast, a high concentration of fluoride in drinking water causes a variety of diseases such as osteoporosis, arthritis, brittle bones, cancer, infertility, brain damage, Alzheimer syndrome, and thyroid disorder, mottling of teeth, neurological damage and interference with DNA synthesis.^{25–28} Fluoride has also been known to cause gastro-intestinal irritation, interfere with carbohydrates, lipids, proteins, vitamins and mineral, and poison kidney function at high doses over short-term exposures in both animals and humans.^{29,30} The most commonly used methods for the defluoridation of water are precipitation,³¹ adsorption,^{32–36} ion-exchange,^{37–42} nano-filtration and electro dialysis,^{43–45} electrocoagulation^{46,47} and reverse osmosis.^{48–49}

However, all these procedures have high operational and sustenance costs and pose threat of secondary pollution.^{50,51} Among the above mentioned methods, the adsorption process is a more attractive method in the context of cost, ease of design and operation and offers satisfactory results. Hence it has been widely used for defluoridation.^{52,53} A range of materials like modified cellulose fiber,⁵⁴ polymer/biopolymer composites,⁵⁵ Fe_2O_3 magnetic nanocomposite,³² bauxite,³³ waste iron oxide³⁴, zeolite³⁵ and multi-walled carbon nanotubes (MWCNTs)³⁶, biosorbents,^{56–58} mixed metal sorbents^{59–61}, nanoadsorbents,^{62,63} and natural materials^{64–70} have been employed for efficient removal of fluoride from aqueous media. For a feasible chemical process to be successful, economics plays an important role. Thus for adsorption, the success depends on how much and how long the solid is capable of retaining the adsorbate at the minimum C/C_0 , which is the maximum activity. In order to overcome the drawbacks of high material cost, energy consumption and environmental contamination, we

strived to achieve a longer breakthrough time, and an efficient, robust, sustainable and reusable mixed metal oxide mesoporous nanoadsorbent for the removal of toxin fluoride ions.

In continuation of our experimental work in improving analytical methods for sensing⁷¹ and removal^{72,88} of fluoride ions and developing sensors for the detection of cations using Au nano-rods⁷³, we have succeeded in our attempt to develop an efficient nanoadsorbent. This is particularly significant in the light of recent reports on toxic fluoride contamination in the rural areas of Rajasthan.⁷⁴ A range of experimental conditions, with initial pH, contact time, adsorbent dose, and temperature were optimized. Various isotherms and kinetic models have been illustrated by means of the experimental data in order to explain the adsorption mechanism.

Experimental

Adsorbent preparation

The Fe–Ce–Ni adsorbent was prepared by co-precipitation method as demonstrated in literature⁴³. Analytical grade $\text{Fe}(\text{NO}_3)_3 \cdot 9\text{H}_2\text{O}$, $(\text{NH}_4)_2[\text{Ce}(\text{NO}_3)_2]$, and $\text{Ni}(\text{NO}_3)_2 \cdot 6\text{H}_2\text{O}$ salts supplied by Sigma–Aldrich were used to prepare the metallic solutions. The other chemicals NaOH, NaF, HCl, and KNO_3 used were of analytical reagents (AR) grade. $\text{Fe}(\text{NO}_3)_3 \cdot 9\text{H}_2\text{O}$ 40.4 g L^{-1} (0.1 M), $(\text{NH}_4)_2[\text{Ce}(\text{NO}_3)_2]$ 109.64 g L^{-1} (0.2 M), and $\text{Ni}(\text{NO}_3)_2 \cdot 6\text{H}_2\text{O}$ 29.08 g L^{-1} (0.1 M) were dissolved in a calculated amount to form a mixed solution. 2 M NaOH solution was added drop wise to the above prepared mixed solution, until the pH of the solution reached 9.5 which lead to precipitation. The obtained precipitate was subsequently centrifuged and washed with deionized water until the pH of the filtrate was in range of 6.5 ± 0.2 . The resulted precipitate was then dried in vacuum and then crushed into fine powder. In order to increase its porosity, the obtained powdered adsorbent was activated in a muffle furnace by gradually increasing the temperature at the rate of 275 K min^{-1} from 353 K up to 773 K for 6 h to blow away all the volatile gases. The powdered adsorbent was allowed to cool down to room temperature in the furnace and then stored in an air tight container for further experiments. A calculated amount of NaF was added to 1 L distilled deionized water to prepare 1000 mg L^{-1} fluoride stock solution. Total ionic strength adjustment buffer (TISAB) was used to get accuracy in readings. All the further experiments fluoride solutions were prepared from the stock solution by suitable dilution methods.

Characterization of adsorbent

The mechanism and extent of fluoride adsorption were determined using various analytical tools. The morphology of surfaces was characterized using field emission scanning electron microscope (SEM) model MIRA3 TESCAN. Energy dispersive X-ray (EDX) analysis of the samples was carried out to determine the mean element proportions of the sample on an Oxford Instrument INCA attached to the FESEM. For EDS analysis an accelerating voltage of 30 kV was used with an acquisition time of about 1 min. An extremely thin vacuum-evaporated carbon coating of samples was done to improve the conductivity of the samples. The Fourier transformed infrared (FTIR) spectral analysis was carried out using FTIR spectrophotometer (Agilent 660, USA). For this all samples were prepared using potassium bromide (KBr) disc method with 2 mg of sample in 100 mg KBr and the spectra were obtained in an IR region between 4000–400 cm^{-1} . Brunauer, Emmett and Teller (BET) analysis was used to determine accurate specific surface of the adsorbent before and after fluoride adsorption by nitrogen monolayer adsorption measured as a function of relative pressure using a fully automated analyzer, model Nova 2000e, Quantachrome Instruments Limited, USA, and using BET equation shown below.⁷⁰

$$\frac{1}{v\left[\left(\frac{p_o}{p}\right) - 1\right]} = \frac{c - 1}{v_m c} \frac{p}{p_o} + \frac{1}{v_m c}$$

where p and p_o are the equilibrium and the saturation pressure of adsorbates at the adsorption temperature, v_m is the monolayer adsorbed gas quantity and c is the BET constant.

A plot of $1/[v(p/p_o) - 1]$ vs p/p_o gives a straight line where p/p_o = relative pressure and v is the adsorbed gas quantity. The data were processed using ORIGIN 6.0. The goodness of fit model was tested by using regression correlation coefficient (R^2). The percentage fluoride removal efficiency was computed from the equation below:

$$\% \text{ Removal} = \frac{(1 - C_o)}{C_t} \times 100 \quad (1)$$

where C_o and C_t are the initial fluoride concentration and fluoride concentration at time t (mg L^{-1}), correspondingly. The fluoride removal efficiency was calculated from following equation:

$$q_t = \frac{(C_o - C_t) v}{m} \quad (2)$$

where q_t is the removal efficiency (mg g^{-1}) at time t , C_o and C_t are the initial fluoride concentration and fluoride concentration at time t (mg L^{-1}), correspondingly.

Batch sorption experiments

The batch adsorption experiments were conducted consecutively to examine the adsorption isotherm of fluoride ions uptake. The adsorption experiments were performed with 250 mL of fluoride ions solution of various concentrations and 0.1 g adsorbent. The contact time was 30 min and the flasks were shaken at 150 rpm in a shaker at 303 K in order to determine the highest adsorption efficiency. 1 mL total ionic strength adjuster buffer (TISAB) solution was added in all the sample solutions to basically mask major chemical interferences in the analyte solution and therefore augment the precision of the readings. In order to study, the effect of initial fluoride concentration on adsorption capacity different fluoride ions solutions were prepared. The pH parameter was checked by preparing different pH solutions using 0.05 M HCl or 0.05 M NaOH. The left over fluoride concentration in the aqueous phase was analyzed by a fluoride ions meter equipped with Orion fluoride ion selective electrode (Thermo Scientific Orion, USA). Finally the solution was filtered out using Whatman filter paper no. 42 and dried in vacuum desiccator for further characterization (BET, FTIR, FESEM, and EDS).

Results and discussion

BET analysis

BET analysis was carried out in order to determine specific surface area, pore size and pore volume before and after fluoride ions adsorption using a completely automated analyzer and the results is shown in Table 1. Surface area was calculated by presuming that the nitrogen adsorbed on the adsorbent formed a monolayer. The specific surface area (N_2 /BET method) and average pore diameter of Fe–Ce–Ni adsorbent is calculated by the isotherm plots and the surface characteristics of adsorbent are tabulated in Table 1. The N_2 adsorption/desorption isotherm curves (Fig. S1†) of developed nanoporous adsorbent can be considered as mixed isotherm, i.e. combination of type I and IV isotherms as a result of the presence of different types of pores (micropores, mesopores) in the adsorbent. While considering the properties of type I isotherm, it can be seen from the curves that the isotherm does not level off below the relative pressure of 0.1, suggesting presence of an appreciable amount of mesopores in addition to micropores as suggested by BET pore size analysis. Analysis of isotherm suggests that adsorption occurred through monolayer-multilayer adsorption. Hysteresis loop in the desorption curve suggests the presence of type IV isotherm showing capillary condensation in mesopores. In capillary condensation the residual pore space which remains after multilayer adsorption has occurred is filled with condensate separated from the gas phase by menisci.

In addition, if the porous material consists of a disordered and inhomogeneous pore system which could result for instance in type H2 hysteresis quite different scanning behavior is expected to be observed. Type H2 hysteresis had been associated with microporous materials contain more complex pore networks consisting of pores with ill-defined shape and wide pore size distribution.^{75–78}

Specific surface area of adsorbent before and after fluoride ions adsorption is estimated using multipoint BET equation in the p/p_0 range of 0.05–0.35 (Fig. 1) which comes out as 436.8 and 457.4 $\text{m}^2 \text{g}^{-1}$ correspondingly. The increase in the surface area demonstrates decrease in pore size which clearly shows the accumulation of fluoride ions by the pores of the developed nanoadsorbent.⁷⁹ An immense change in the structure has led to the increase in surface area of the adsorbent throughout the adsorption of the fluoride ions.^{79–82} Dubinin–Atakhov (D–A) equation⁸⁰ was applied consecutively to demonstrates pore size distributions and pore characteristics, and the corresponding plots are shown in Fig. 2. D–A pore radii before and after fluoride ions adsorption were found to be 15.10 Å and 14.30 Å correspondingly (Fig. 2). The decrease in pores radii clearly shows the adsorption of fluoride ions inside the pores of the adsorbent materials which in turn increases the surface area of the adsorbent. The results of present study establish that as the surface area increases the pores radii decrease (Table 1).

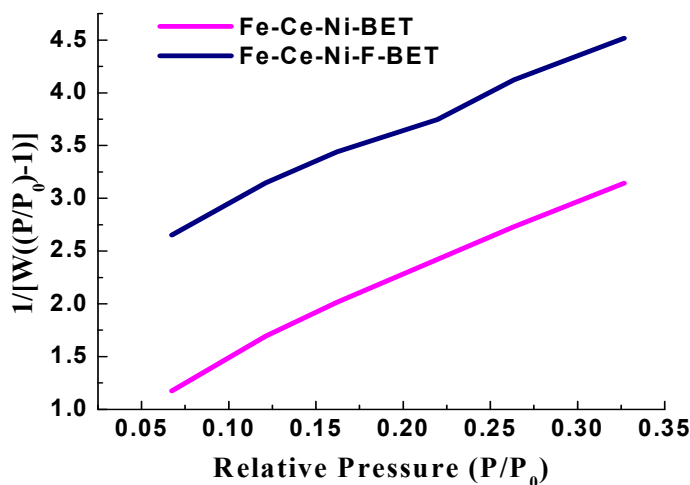


Fig. 1 Brunauer, Emmett and Teller surface area plots where magenta line is before fluoride absorption and navy blue line is after fluoride adsorption.

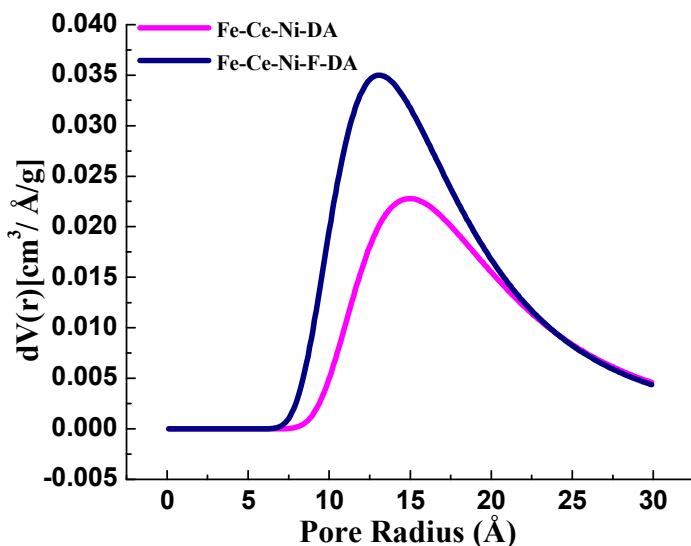


Fig. 2 Dubinin–Astakhov plots for pore radius where magenta curve is before fluoride adsorption and navy blue curve is after fluoride adsorption.

Table 1 The surface area, pore size and pore volume of the adsorbent determined before and after fluoride adsorption

Adsorbent	Surface Area ($\text{m}^2 \text{g}^{-1}$)	Pore Size (Å)	Pore Volume (cc g^{-1})
Before fluoride adsorption	436.8	15.10	0.511
After fluoride adsorption	457.4	14.30	0.501

FTIR analysis

The FTIR spectra of the Fe–Ce–Ni nanoadsorbent before and after fluoride adsorption are demonstrated in Figs. S2† and S3†, respectively. From the Fig. S2†, the broad band at 3410 cm^{-1} can be consigned to the stretching vibration of adsorbed water, and the peak at 1634 cm^{-1} has been ascribed to the bending vibration of OH group⁸³ of the Fe–Ce–Ni nanoadsorbent. The peaks observed at 924 cm^{-1} , 532 cm^{-1} and 459 cm^{-1} are attributed to the vibrations of mixed metals oxides. The strong peak at 1385.8 cm^{-1} demonstrates the anti-symmetric stretching of NO_3^- groups.⁸⁴ A substantial diminish in the intensity of the band at 1385.8 cm^{-1} implies that fluoride ions adsorption by the adsorbent to some extent occurred by ion exchange with nitrate. It can be clearly seen that the emergence of bands at 924.1 cm^{-1} and 532.0 cm^{-1} is the characteristics of Ce–O and Ni–O bonds, respectively in the adsorbent.⁸⁵ A characteristic band observed at 459.4 cm^{-1} can be attributed to the Fe–OH

bending vibrations.⁸⁵ The shifting of the bands after fluoride adsorption from 3410 cm^{-1} to 3395.8 cm^{-1} and from 1634 cm^{-1} to 1627.9 cm^{-1} with subsequent decrease in intensity can be attributed to the interaction of fluoride ions with the hydroxyl groups on the adsorbent.⁸⁶ The shift in the IR peaks from 924.1 cm^{-1} , 532.0 cm^{-1} and 459.4 cm^{-1} to 930.2 cm^{-1} , 531.3 cm^{-1} and 459.2 cm^{-1} after fluoride adsorption can be associated with interaction of the fluoride ions with the metal oxide bonds.

FESEM and EDS analyses

The surface morphology of nanoadsorbent before and after the modification was characterized using SEM analysis. Figs. 3 and 4 show the FESEM images of the adsorbent before and after fluoride adsorption, respectively. The FESEM photographs of adsorbent before fluoride uptake are illustrated no precise shape or crystalline constitution. The surface morphology of the adsorbent rather appears like flakes and the particles have irregular shapes. It can also be seen from the images that the surface texture of the adsorbent is porous having holes and minute cavities on the surface, thus increasing the contact area facilitating the pore diffusion during adsorption. After adsorption of fluoride, a reduction in the pore size was observed which may be due to sorption of fluoride onto the adsorbent (Fig. 4). EDS measurements presented in Fig. 5 designates that the main components of the adsorbent are Ce, Fe, Ni and O peaks. The chemical composition from EDS analysis confirmed that the developed nanoadsorbent has Fe (17.37%), Ce (34.43%), Ni (17.26%), and O (30.94%). No other peak was detected in the EDS pattern indicating the purity of the developed adsorbent. The presence of fluoride ions peak in EDS spectrum after fluoride adsorption (Fig. 6) including other elements of adsorbent confirmed fluoride adsorption by adsorbent.

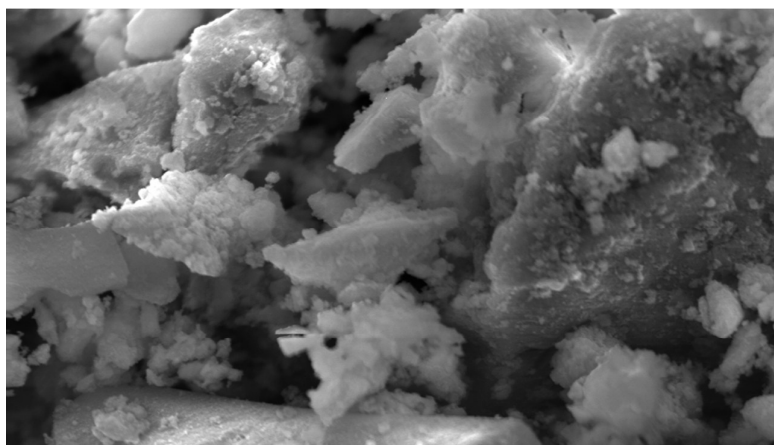


Fig. 3 SEM image of Fe–Ce–Ni nanoadsorbent before fluoride adsorption.

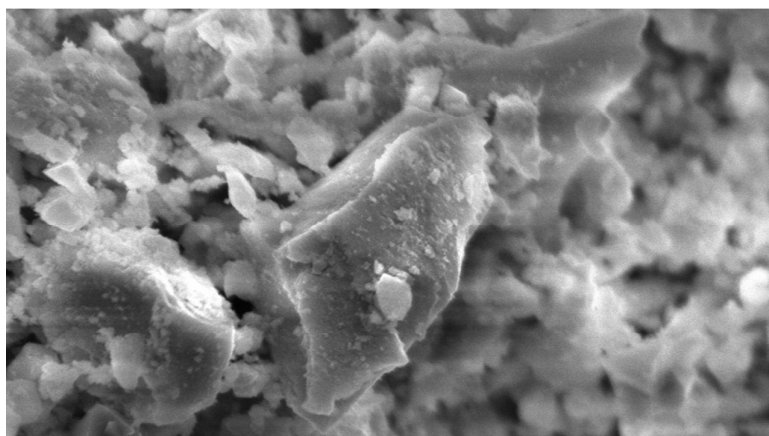


Fig. 4 SEM image of Fe–Ce–Ni nanoadsorbent after fluoride adsorption.

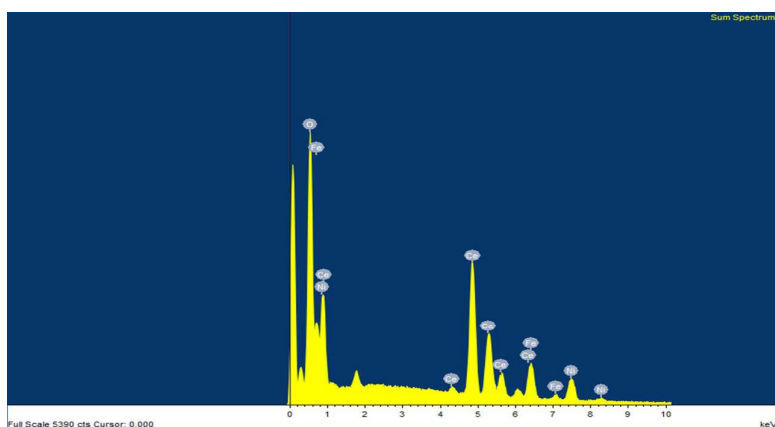


Fig. 5 EDS spectrum of Fe–Ce–Ni nanoadsorbent before fluoride adsorption.

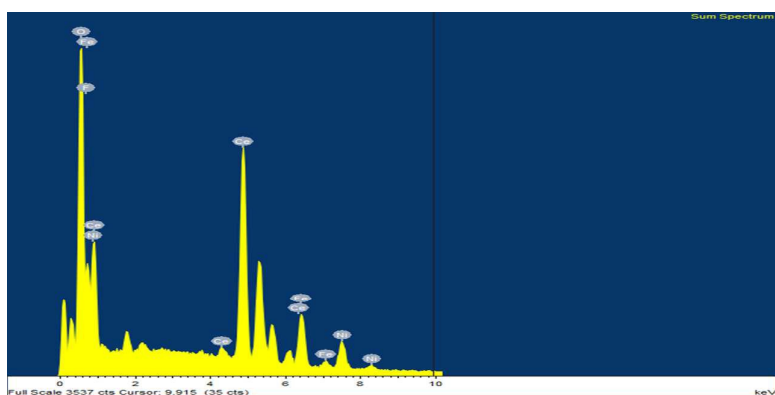


Fig. 6 EDS spectrum of Fe–Ce–Ni nanoadsorbent after fluoride adsorption.

Equilibrium modeling

In order to determine equilibrium adsorption capacity and capability of adsorbent for fluoride ions at pH 7.0 (± 0.1), and at three different temperatures (303, 313 and 323 K), the experimental isotherm data are illustrated in Figs. S4†, 7, S5†, and 8. The precise correlation between the adsorbent concentration and extent of fluoride adsorption on adsorbent surface at a particular temperature was estimated by means of four different isotherms specifically Langmuir, Freundlich, Temkin and Dubinin–Radushkevich. The mathematical expression of Langmuir and Freundlich isotherm models in their linear form are illustrated in Table 2.^{87–91} From Langmuir isotherm, C_e is the equilibrium concentration of adsorbate (mg L^{-1}), q_e is the amount of fluoride adsorbed per gram of the adsorbent at equilibrium (mg g^{-1}), Q^0 is maximum monolayer coverage capacity (mg g^{-1}) and b is Langmuir isotherm constant (L mg^{-1}) and in Freundlich isotherm k_F is Freundlich isotherm constant (mg g^{-1}), and n is the adsorption intensity. From Temkin isotherm A_T is the Temkin isotherm equilibrium binding constant (L g^{-1}), b_T is the Temkin isotherm constant (kJ mol^{-1}), R is the ideal gas constant ($8.314 \text{ J mol}^{-1} \text{ K}^{-1}$), and T is absolute temperature (K) and in D–R isotherm q_s is theoretical isotherm saturation capacity (mg g^{-1}), K_{ad} is D–R isotherm constant ($\text{mol}^2 \text{ kJ}^{-2}$) and ϵ is D–R isotherm constant.

A linear plot between $1/C_e$ and $1/q_e$ demonstrated the Langmuir isotherm as shown in Fig. S4†.^{92,93} The values of Q^0 and b were calculated from the slope and intercept of the plot and the results are listed in Table 3. A raise in adsorption capacity as demonstrated by increased Q^0 values with temperature implied the fluoride uptake is mainly by means of chemisorption mechanism. Langmuir isotherm assumes no cooperation among the adsorbed molecules and the adsorption occurred in a monolayer. Freundlich isotherm assumes that adsorbent has surfaces of varied affinities or adsorption on heterogeneous surfaces where adsorption on the stronger binding sites occurs first; after that the binding strength decreases due to increase in degree of site occupation.^{88,89} A linear plot between $\log q_e$ and $\log C_e$ demonstrated the Freundlich isotherm as shown in Fig. 7. The values of Freundlich isotherm constants $1/n$ and k_F were calculated from the slope and intercept of the plot and the results are shown in Table 3. The values of $1/n$ came out in between 0 and 1 and the higher value of ‘ n ’ illustrated favourable conditions for adsorption.⁹⁴ The applicability of Freundlich isotherm illustrates reversible nature of adsorption which is not constrained to the creation of monolayer and the heterogeneous nature of the adsorbent sites.^{95,96} An increased value of intensity of adsorption (n) and adsorption energy (k_F) from Freundlich data with the increase

in temperature also supported the endothermic nature of the adsorption process. The Temkin adsorption isotherm demonstrates adsorbent–adsorbate interaction. The isotherm presumes that the decline in heat of adsorption linearly with the sorption coverage interactions is a result of adsorbent–adsorbate interaction. A linear plot between q_e and $\ln C_e$ demonstrated Temkin isotherm as shown in Fig. S5†. The values of Temkin isotherm constants A_T and b_T were calculated from the intercept and slope of the plot and the results are tabulated in Table 4. The highest value of heat of adsorption calculated using Temkin model is $16.17 \text{ kJ mol}^{-1}$ at 323 K. Furthermore, to demonstrate the adsorption nature, D–R isotherm was studied. A linear plot between $\log q_e$ and $\log C_e$ demonstrated D–R isotherm as shown in Fig. 8 with correlation coefficient (R^2), 0.983. D–R isotherm constant K was calculated from the slope of the plot. The value of D–R isotherm constant (K_{ad}) at 303, 313 and 323 K was established to be -0.0017 , -0.0016 and $-0.0015 \text{ mol}^2 \text{ kJ}^{-2}$ respectively (Table 4). By the help of D–R isotherm constant values, mean free energy of adsorption (E), which is the free energy change occurred due to the transfer of 1 mol of ions in the solution to the adsorbent surface from infinity, was estimated using the relation as shown below:

$$E = (-2K_{ad})^{-1/2}$$

The highest mean free energy of adsorption $12.04 \text{ kJ mol}^{-1}$ was established at 323 K. Since the value of E is in between $8\text{--}16 \text{ kJ mol}^{-1}$, then the adsorption can be well elucidated by an exchange of ions.⁹⁷ Hence, in order to estimate the best fitting of isotherm equations to experimental data, the coefficient of regression (R^2) and Standard Deviation (SD) values were compared. It is established that both Freundlich as well as D–R isotherm models are the most appropriate models in order to illustrate the adsorption phenomenon in the present investigation.

Table 2 Isotherm models and their linear forms

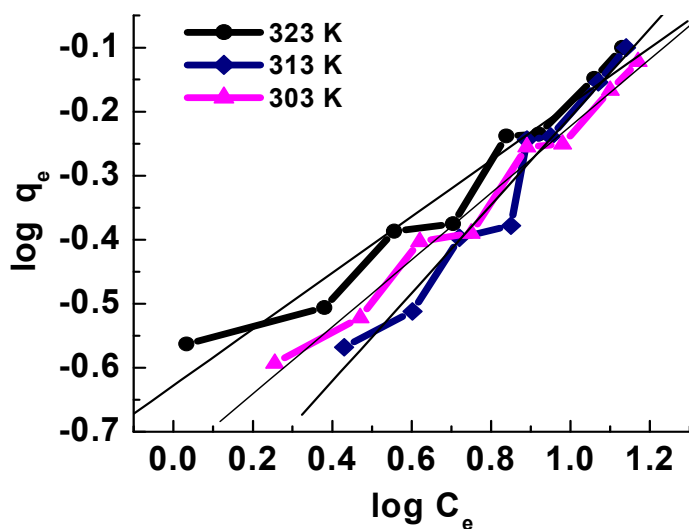
Isotherm	Linear form	Plot
Freundlich $q_e = k_F C_e^{1/n}$	$\log q_e = \log k_F + 1/n \times \log C_e$	$\log q_e$ vs $\log C_e$
Langmuir $q_e = Q^0 b C_e / (1 + b C_e)$	$C_e / q_e = (1/Q^0 b) + (C_e / Q^0)$	$1/q_e$ vs $1/C_e$
Temkin $q_e = \frac{RT}{b_T} \ln(A_T C_e)$	$q_e = \frac{RT}{b_T} \ln(A_T) + \frac{RT}{b_T} \ln(C_e)$	q_e vs $\ln(C_e)$
D–R $q_e = (q_s) \exp(-K_{ad} \varepsilon^2)$	$\ln(q_e) = \ln(q_s) - (K_{ad} \varepsilon^2)$	$\ln(q_e)$ vs ε^2

Table 3 The values of Freundlich and Langmuir isotherms constants

Temperature (K)	Langmuir isotherm				R^2	Freundlich isotherm			
	$1/Q^0$	Q^0	$1/b$	b		k_F	$1/n$	n	R^2
303	0.0080	125.0	0.6	1.66	0.953	31.8	0.069	14.4	0.982
313	0.0050	200.0	0.4	2.50	0.945	31.8	0.067	14.9	0.983
323	0.0035	285.7	0.25	4.00	0.937	31.9	0.066	15.1	0.981

Table 4 The values of Temkin and Dubinin–Radushkevich isotherms constants

Temperature (K)	Temkin isotherm			Dubinin–Radushkevich isotherm			
	b_T (kJ mol ⁻¹)	A_T (L g ⁻¹)	R^2	K_{ad} (mol ² kJ ⁻²)	q_s (mg g ⁻¹)	ϵ	R^2
303	14.23	0.86	0.952	-0.0017	0.30	717	0.982
313	15.39	0.91	0.959	-0.0016	0.76	817	0.983
323	16.17	0.94	0.965	-0.0015	0.56	931	0.981

**Fig. 7** Freundlich isotherm outlines of the fluoride adsorption by nanoadsorbent.

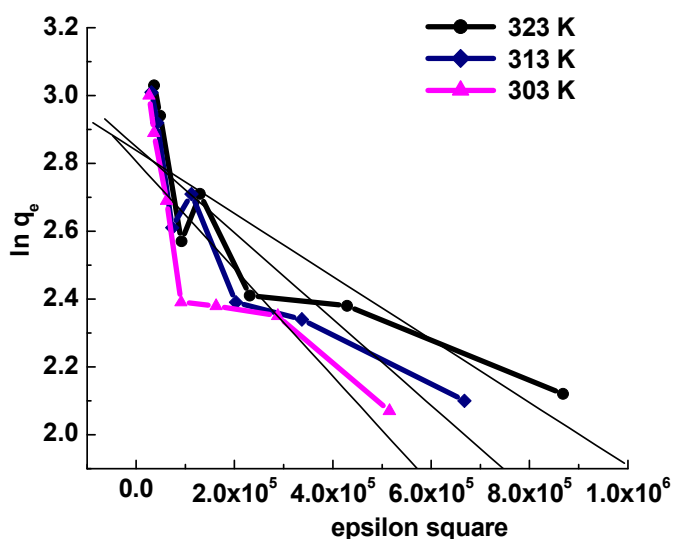


Fig. 8 Dubinin–Radushkevich isotherm outlines of the fluoride adsorption by nanoadsorbent.

Reaction–based models

In order to define the adsorption efficiency, a characteristic kinetics study regarding the fluoride uptake by the Fe–Ce–Ni nanoadsorbent was performed. The adsorption kinetics has been studied with various mathematical expressions for instance pseudo–first–order, pseudo–second–order, and intra–particle diffusion.^{98–102}

The mathematical expressions of various models are represented in Table 5. The irreversible nature of the adsorption of solid/liquid systems is described by the pseudo–first–order mathematical equation, where q_e and q_t signify the amount of fluoride adsorbed (mg g^{-1}) at equilibrium and at time ‘t’, correspondingly and k_F (min^{-1}) being the rate constant of pseudo–first–order reaction. A linear plot of $\log(q_e - q_t)$ vs t, produced a straight line and values of both q_e and k_{ad} were determined by the intercept and slope of the curve, correspondingly (Fig. S6†). The chemisorption as one of the factors controlling the sorption kinetics is expressed by pseudo–second order equation, where ‘h’ signifies the rate constant for pseudo–second–order reaction ($\text{g mg}^{-1} \text{min}^{-1}$). The linear plot of t/q_t vs t for the kinetic data produced a straight line and the values of both q_e and h, were determined from the slope and intercept, correspondingly (Fig. 9).^{101,102} The Weber–Morris intra–particle diffusion expression is also demonstrated, where k_{id} is the intra–particle diffusion constant ($\text{mg g}^{-1} \text{min}^{-1/2}$) and C being the intercept of the plot.⁹⁸ The linear plot of q_t vs $t^{1/2}$ for the kinetic data produced a straight line and the values of both k_{id} and C, were determined from the slope

and intercept, correspondingly from Fig. 10, where the intercept C value demonstrated the thickness of boundary layer i.e., the resistant to the external mass transfer.

Intra-particle diffusion expression demonstrates that the diffusion process possibly influenced in the rate limiting step, because through an increase in the temperature the k_{id} amplified, demonstrating the endothermic nature of the adsorption process. Higher the value of intercept higher will be the external resistant to mass transfer. The high value of correlation coefficient (R^2) as 0.994 demonstrates the relevancy of the pseudo-second-order kinetic model as shown in Table 6.¹⁰³

The Freundlich adsorption isotherm and pseudo-second-order kinetics, combination reveals that the fluoride uptake takes place by means of chemisorption processes through monolayer formation on the heterogeneous adsorbent sites of Fe-Ce-Ni nanoadsorbent. The existence of intra-particle diffusion in the adsorption process implies that intra-particle diffusion commences on succeeding dissemination of the complete adsorbent active sites with fluoride ions.

Table 5 Reaction based kinetic models and their linear expressions

Reaction-based Kinetic model	Linear form	Plot
Pseudo-first-order	$\log(q_e - q_t) = \log q_e - (k_{ad}/2.303)t$	$\log(q_e - q_t)$ vs t
Pseudo-second-order	$(t/q_t) = (1/h) + (t/q_e)$	t/q_t vs t
Weber-Morris model	$q_t = k_{id} t^{1/2} + C$	q_t vs $t^{1/2}$

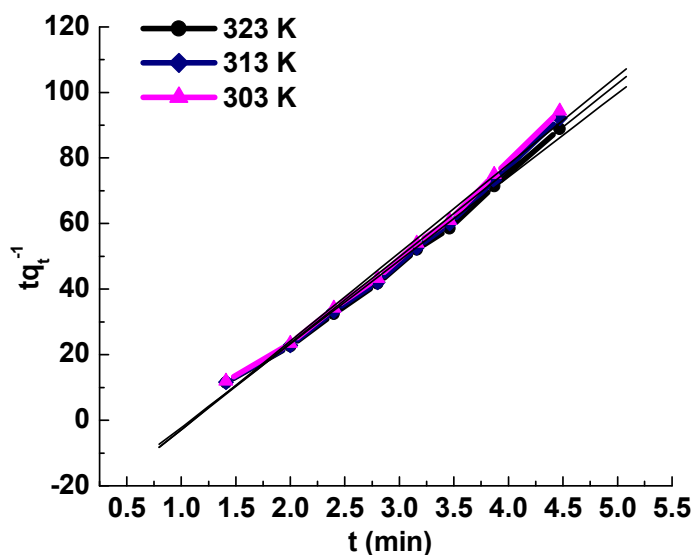


Fig. 9 Pseudo-second-order plots of the fluoride adsorption by nanoadsorbent.

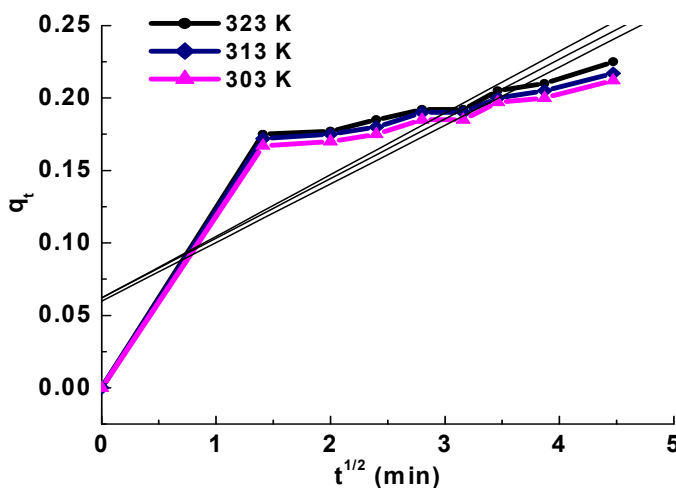


Fig. 10 Weber–Morris (Intra–particle diffusion) plots of the fluoride adsorption by nanoadsorbent.

Table 6 Kinetic parameters for three types of reaction-based kinetic models

Temperature (K)	Pseudo–first–order rate constant			Pseudo–second–order rate constant			Weber–Morris model rate constant		
	k_{ad}	q_e	R^2	h	q_e	R^2	k_{id}	C	R^2
303	0.126	11.2	0.920	0.034	0.037	0.992	0.040	0.059	0.738
313	0.101	11.4	0.917	0.034	0.037	0.994	0.041	0.062	0.732
323	0.066	11.8	0.969	0.039	0.039	0.992	0.042	0.062	0.745

Thermodynamic analysis

Thermodynamics parameters such as the changes of Gibbs free energy ΔG^0 , enthalpy ΔH^0 and entropy ΔS^0 for the adsorption of fluoride on adsorbent are calculated wherein R is the ideal/universal gas constant ($8.314 \text{ J mol}^{-1} \text{ K}^{-1}$), T is the absolute temperature (K), and B_1 is the Langmuir equilibrium constant. The results are shown in Table 7.^{104,105} The Gibbs free energy change values (kJ mol^{-1}) calculated using the Langmuir equilibrium constant (B_1), obtained by linear analysis, are -1.45 and -0.95 , and -0.410 respectively at 323, 313 and 303 K as tabulated in Table 7. The Gibbs free energy change values obtained for the adsorption of fluoride ions on adsorbent indicated the adsorption process is spontaneous in nature, and

the spontaneity of adsorption reaction increases with temperature. Again, the high positive ΔH^0 value (+14.99 kJ mol⁻¹) indicates the adsorption of fluoride is endothermic as shown in Table 7. The calculated positive ΔS^0 value (+85 J mol⁻¹ K⁻¹) (Table 8) indicates the increase in entropy indicating the adsorption phenomenon takes places with increasing number of molecules/ions at solid–liquid interface.^{106–108} The positive value of ΔS^0 also indicates the stable and irreversible nature of the adsorption process.¹⁰⁹ This is presumably due to the increase in solvent molecules at the solid–liquid interface because when hydrated fluoride ions adsorb onto the solid surface, the water molecules are released at the solid–liquid interfacial position in terms of moles of this is greater than the fluoride ions being adsorbed by the solid.

Table 7 Thermodynamic parameters and their corresponding equations

Thermodynamic parameter	Thermodynamic equation
ΔG^0	$\Delta G^0 = -2.303RT \log_{10} B_1$
ΔH^0	$\log_{10} B_1(T_2) - \log_{10} B_1(T_1) = -(\Delta H^0/2.303R)[1/T_2 - 1/T_1]$
ΔS^0	$\Delta S^0 = (\Delta H^0 - \Delta G^0)/T$

Table 8 Thermodynamic parameters value of adsorbent

Thermodynamic parameter	Temperature (K)	Fe–Ce–Ni nanoadsorbent
ΔG^0 (kJ mol ⁻¹)	323	-1.45
	313	-0.95
	303	-0.41
ΔH^0 (kJ mol ⁻¹)		+14.99
ΔS^0 (J mol ⁻¹ K ⁻¹)		+85.0

Point of zero charge (PZC) analysis

Behavior of potential–determining ions (H⁺ and OH⁻) and electrolyte concentrations (ionic strength) determines surface charge in a system. The surfaces may have net negative, or positive, or no charge, depending on nature of the adsorbent. The pH showing the overall unit particle charge zero is known the point of zero charge (PZC). It is one of the most significant factor apply to show variable charge surfaces. If the pH of an adsorbent is more than its PZC

then the adsorbent surface will possess a unit negative charge and predominantly demonstrate a capability to exchange cations. If the pH of an adsorbent is beneath its PZC then the adsorbent surface will exhibit an overall positive charge and possessively show anion exchange behavior. From a variety of methods, potentiometric titration was used for determination of the PZC on nanoadsorbent which demonstrates alteration in surface potential with alteration in the activities of H^+ and OH^- ions. From Fig. S7†, it can be seen that the PZC of the Fe–Ce–Ni nanoadsorbent works out 8.9 which demonstrates the overall positive charge on the adsorbent surface showing anion exchange behavior.

Effect of pH

Fig. 11 demonstrates the consequences of solution pH on adsorption of analyte on adsorbent at 303 K. With increasing pH from 2.0–7.0, the rate of fluoride uptake by adsorbent from aqueous solution amplified and further increase in pH from 7.0 onward decreased the adsorption behavior. Adsorbent surface acts as positively charged surface in acidic pH as a result of the following reaction any (i) or (ii).



Existing fluoride ions in the acidic medium combine on the positively charged adsorbent surface of the adsorbent by means of columbic forces either through outer (iii) or inner sphere (iv) complex reaction mechanism.



Diminished fluoride uptake in strongly acidic medium may be due to the formation of the HF by means of the reaction (v) and hence there is a diminished existing fluoride ions concentration meant for fluoride uptake.



On further increasing pH above 7 there is diminished fluoride uptake as a result of more availability of fluoride ions due to concentration reaction (V) shift on the left side. The reduced fluoride uptake may also be due to alteration in the surface nature of the adsorbent. Above pH 7 the surface of the adsorbent becomes negatively charged and the competition of the OH^- ions for the same active sites on the adsorbent surface.^{110–112} As a result the most favorable pH range attained for fluoride uptake is 5.0–7.0 and all the further experiments

were conducted at pH 7 (± 0.1) characteristically in drinking water pH range as shown in Fig 11.

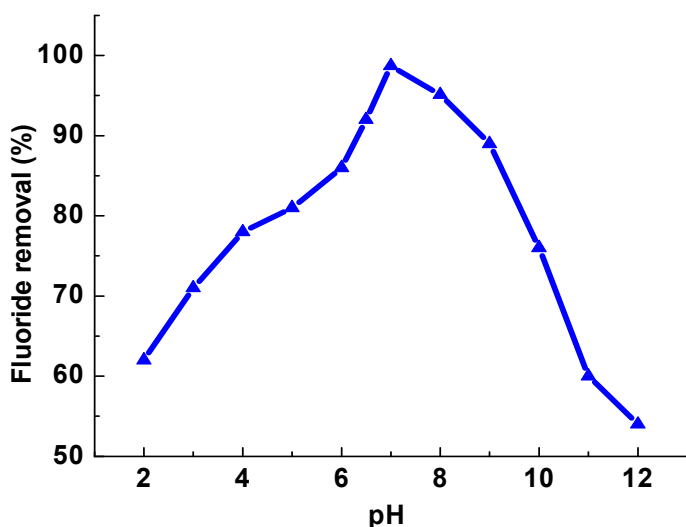


Fig. 11 Effect of pH on fluoride adsorption (Adsorbent dose: 0.4 g L^{-1} , initial F^- concentration: 10 mg L^{-1} , temperature: 303 K , time: 30 min).

Effect of adsorbent dose

The effect of variation of adsorbent doses on the fluoride uptake at optimum pH of 7.0 with a contact time of 30 min and initial fluoride ions concentration 10 mg L^{-1} was analyzed and the results are depicted in Fig. 12. The quantity of adsorbent appreciably controls the degree of fluoride uptake. The increase in adsorption capacity with increase in amount of adsorbent is caused by the accessibility of higher quantity of fluoride ions for every unit mass of adsorbent.^{113,114} However, additional raise in adsorbent amount does not cause any significant enhancement in fluoride uptake due to saturation of the adsorbent surface sites.^{115,116} The highest percentage fluoride removal was estimated to be 98.7% with an adsorbent dose of 0.4 g L^{-1} of fluoride solution, which is very good adsorption efficiency. Consequently 0.4 g L^{-1} as optimum dose of the adsorbent was chosen for further experimentation.

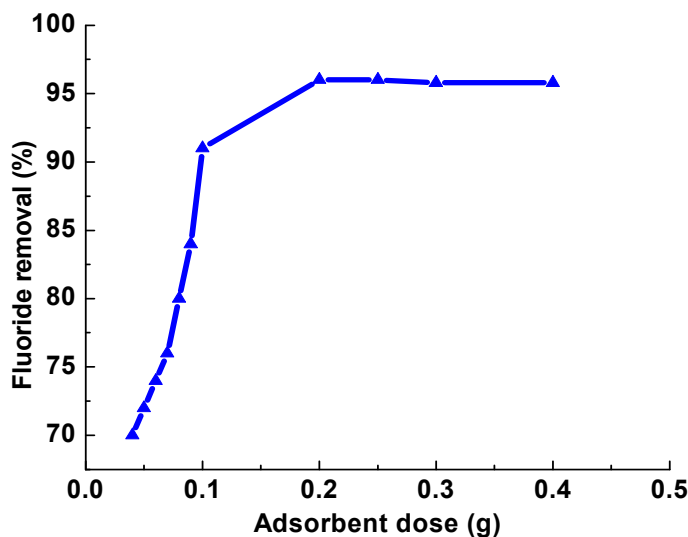


Fig. 12 Effect of adsorbent dose on fluoride adsorption (Initial F^- concentration: 10 mg L^{-1} , pH: 7, temperature: 303 K, time: 30 min).

Effect of contact time

The variation of defluoridation efficiency with contact time was demonstrated by changing the contact time from 2–45 min with the adsorbent dose 0.4 g L^{-1} , pH 7 and initial fluoride concentration of 10 mg L^{-1} and the results in form of percentage fluoride removal are presented in Fig. 13. A careful examination of the adsorption outline illustrates that percentage fluoride removal enhanced on increasing contact time during the first 20 min where most fluoride uptake occurred. Then there was a slow adsorption period up to 30 min which may be due to the attainment of equilibrium of the adsorption process and no consequent rise in the adsorption took place beyond 30 min. This can be explained by saying that at first the entire adsorbent site was accessible for the fluoride uptake and also initially a high solute concentration gradient was present. Further increase in contact time does not cause any appreciable rise in adsorption efficiency due to the saturation of adsorbent sites which leads to decrease in the number of available adsorbent sites and diminished amount of the residual fluoride ions in the solution.^{117–120}

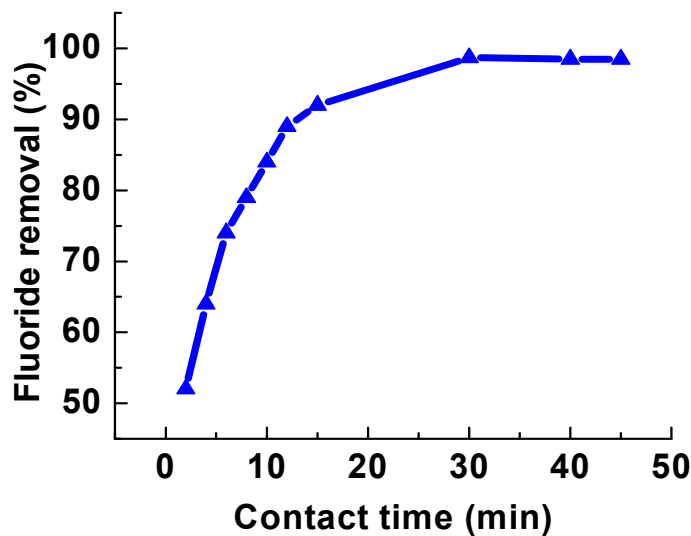


Fig. 13 Effect of contact time on fluoride adsorption (Adsorbent dose: 0.4 g L^{-1} , initial F^- concentration: 10 mg L^{-1} , pH: 7, temperature: 303 K).

Effect of initial fluoride ions concentration

The variation of defluoridation efficiency with initial fluoride ions concentration was demonstrated by changing the initial fluoride ions concentration from $5\text{--}45 \text{ mg L}^{-1}$ with the adsorbent dose 0.4 g L^{-1} , pH 7 and contact time of 30 min and the results in form of percentage fluoride removal are presented in Fig. 14. There was a decrease in adsorption efficiency with the augmentation in the initial fluoride ions concentration. This can be explained by the presence of more fluoride ions per unit number of adsorbent sites which leads to saturation of the coordination sites.^{121,122}

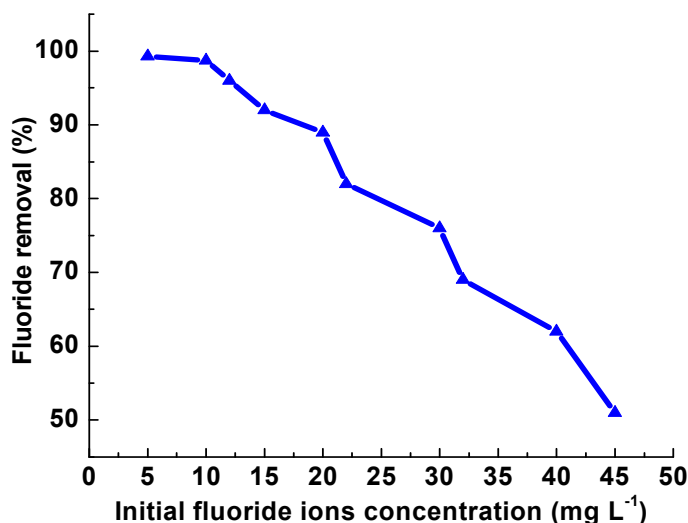


Fig. 14 Effect of initial fluoride ions concentration on fluoride adsorption (Adsorbent dose: 0.4 g L^{-1} , pH: 7, temperature: 303 K, time: 30 min).

Comparison of fluoride adsorption efficiency and optimum pH for various adsorbents

The comparison of adsorption efficiency of various adsorbents and other parameters for fluoride removal with the present work is given in Table 8. The developed nanoadsorbent in the present study is a better quality adsorbent with respect to other adsorbents studied in the literatures. Thus the developed nanoadsorbent is a promising adsorbent for fluoride removal from aqueous solution under optimum conditions. The significantly high adsorption efficiency of the nanoadsorbent is significantly high as compared to the other adsorbents at normal drinking water pH range.^{83,123–133} Additionally, the synthesized nanoadsorbent displayed a higher surface area as compared to the adsorbents studied in the literature illustrating its high porosity and adsorbing efficiency at normal water pH 7.0.

Table 9 A comparative evaluation of fluoride adsorption efficiency of developed nanoporous adsorbent with some reported literature data

Adsorbent	Adsorption efficiency (mg g^{-1})	pH	References
Iron–zirconium hybrid oxide	8.21	7	120
Iron–aluminum mixed oxide	17.73	6 ± 0.2	121

Hydrated iron(III)–aluminum(III) chromium(III) ternary mixed oxide (HIACMO)	31.89	5.6	122
Al–Ce hybrid adsorbent	27.5	12	123
Fe–Al–Ce nanoadsorbent	5.9	5.5	124
Granular zirconium–iron oxide (GZI)	9.80	6	125
Mg–Al–LDH nanoflake impregnated magnetic alginate beads (LDH–n–MABs)	61.8	5.0	83
Basic aluminum sulfate and graphene hydrogel (BAS@GHG)	68.9	7.0	126
Hollow MgO microspheres	120.0	7.0	127
Aluminium oxide hydroxide (nano–AlOOH)	62.5	7.0	128
Electrospun alumina nanofibers	1.2	7.0	129
Zr(IV)–poly(acrylamide) magnetic composite	124.5	1–9	130
Fe ₃ O ₄ @Al(OH) ₃ nanoparticles	88.5	6.5	131
La alginate bead	197.2	4.0	132
Mn–Ce binary oxide	137.5	6.0	133
Fe–Ce–Ni nanoadsorbent	285.7	7.0 (±01)	Present work

Effect of co-existing ions

Natural water resources may include various anions for instance Cl^- , NO_3^- , SO_4^{2-} , CO_3^{2-} , HCO_3^- , and PO_4^{3-} in addition to F^- which may have affinity for the same active sites on the adsorbent as reported previously.^{134–136} These co-existing anions thus may result in the reduced removal efficiency; hence it is necessary to study the influence of these anions on fluoride uptake. Normally ground water has natural concentration of these anions as: Cl^- : 0–0.0028 M; NO_3^- : 0–0.0008 M; SO_4^{2-} : 0–0.0104 M; HCO_3^- : 0–0.0065 M; PO_4^{3-} : 0– 5.2×10^{-5} M. A series of experiments were carried out for fluoride uptake in presence of the above mentioned anions with three different concentrations and the results are displayed in Fig. 15. From the figure, it is clear that there is no considerable alteration in adsorption aptitude in the presence of Cl^- (0–0.1 M), NO_3^- (0–0.1 M), SO_4^{2-} (0–0.1 M), CO_3^{2-} (0–0.1 M), HCO_3^- (0–0.1 M), and PO_4^{3-} (0–0.1 M) while presence of SO_4^{2-} , CO_3^{2-} , and PO_4^{3-} in elevated concentration of 0.1 M reduced the fluoride uptake efficiency. Among all the present anions PO_4^{3-} in

solution demonstrated a significant decline in fluoride uptake, as reported in the literature.^{137–139} The decline in fluoride uptake could possibly be as a result of the competition between fluoride and PO_4^{3-} for the same active sites on the adsorbent.

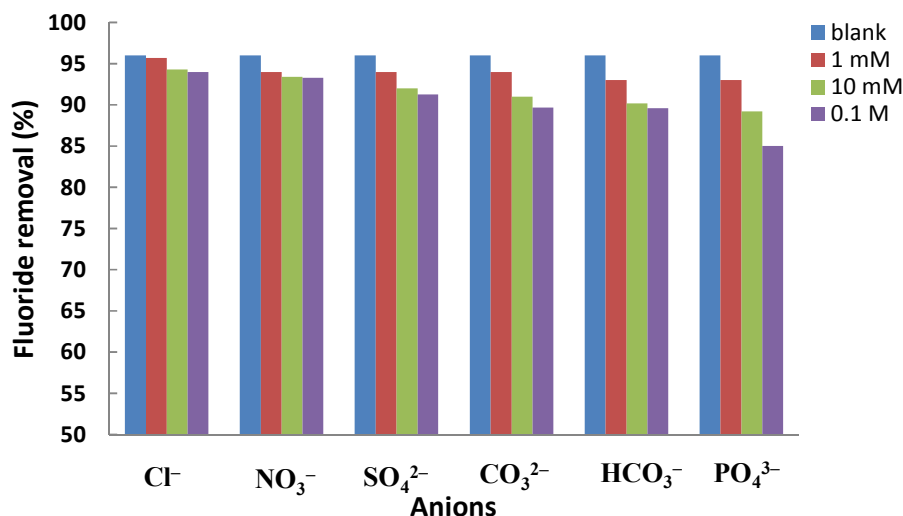


Fig. 15 Effect of co-existing ions. (Adsorbent dose: 0.4 g L^{-1} , concentration of F^- : 10 mg L^{-1} , pH: 7, temperature: 303 K , time: 30 min).

Desorption and reuse efficiency

In order to check the economical viability of the developed nanoadsorbent, the nanoadsorbent was regenerated and reusable capacity of this was checked in several cycles of adsorption process. Firstly, the material was subjected to adsorption process at an initial fluoride ions concentration of 10 mg L^{-1} , in order to examine the desorption efficiency of the adsorbent. The fluoride loaded adsorbent was redeveloped by means of HCl and NaOH. The regeneration of the adsorbent was fairly small in acidic pH, while in alkaline pH efficient leaching of the loaded adsorbent took place. The NaOH concentrations were varied from 0–12%. About 95% of the fluoride loaded adsorbent was desorbed at 4% NaOH concentration. Under similar initial conditions adsorption–desorption cycles were carried out 5 times. In fifth cycle, the adsorbent capacity reduced to 48% from 98.7% as shown in Fig. 16. Accordingly, the investigation reveals that the Fe–Ce–Ni nanoadsorbent can be reused up to five times with considerable efficiency. Adsorption–desorption studies on developed nanoadsorbent ensured its long-term operational stability and recyclability. The stability testing confirmed that the used nanoadsorbents could be easily regenerated with 4% NaOH solution and no significant loss of adsorption capacity were observed after three adsorption–

desorption cycles, suggesting high stability of adsorbent in extremely acidic and alkaline solutions.

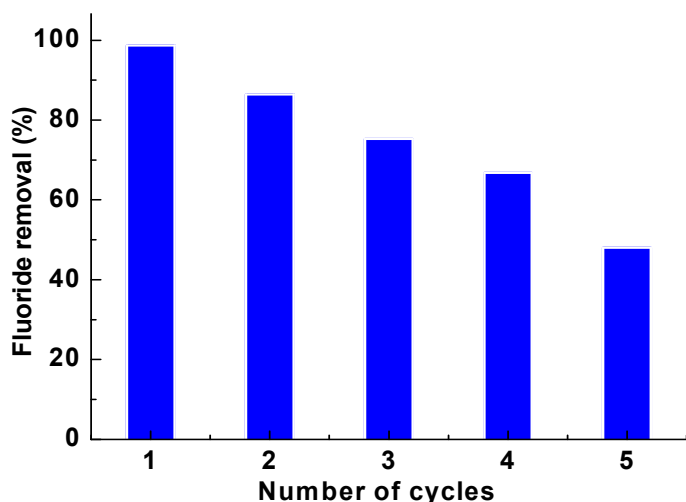


Fig. 16 Adsorption and desorption cycles. (Adsorbent dose: 0.4 g L^{-1} , concentration of F^- : 10 mg L^{-1} , pH: 7, temperature: 303 K , time: 30 min).

Potential applications

A wide variety of adsorbents have been frequently employed at a fluoride concentration beneath 5 mg L^{-1} . Consequently, for 1 m^3 of aqueous solution, the mass of the adsorbent, required to reduce fluoride ions concentration from $5\text{--}1 \text{ mg L}^{-1}$, is evaluated employing following mass balance equation¹⁴⁰:

$$VC_0 = mq_e + VC_e \quad (3)$$

where C_e is the equilibrium concentration of adsorbate (mg L^{-1}), q_e is the amount of fluoride adsorbed per gram of the adsorbent at equilibrium (mg g^{-1}) and C_0 , C_e , and V are 5 , 1 mg L^{-1} , and 1 m^3 , correspondingly.

The mass of the adsorbent obtained from eq (3) is 1.87 kg , which is 4.01 and 1.5 times smaller than that of the AIC-300 carbon (7.5 kg)¹⁴⁰ and aligned carbon nanotubes (2.7 kg)¹⁴¹, correspondingly. Evidently, the proposed adsorbent is highly appropriate for fluoride uptake. Briefly, the superior adsorption efficiency, and cost effectiveness indicate that Fe-Ce-Ni is a suitable nanoadsorbent for fluoride uptake.

Column studies

In order to check field applicability and better practical effectiveness of the synthesized nanoadsorbent, the column study using real water samples was carried out. For this experiment we prepared a sand column with 0.4 g nanoadsorbent. In this order suitability of water in terms of pH, Electrical Conductivity (EC), Total Dissolved Solids (TDS), Dissolved Oxygen (DO), fluoride, chloride, phosphate, sulphate, carbonate, bicarbonate, and nitrate from influent and effluent samples was tested. The values of tested water quality parameters before and after treatment are tabulated in Table S1†. In addition, we also analyzed robustness of the developed nanoadsorbent by leach-out effect in elute with the help of Atomic Absorption Spectroscopy (AAS) before and after treatment. It was found that there was an increase in DO (6.7–7.3 mg L⁻¹), a significant extent of phosphate was removed from influent water and rest of water quality parameters were in the range of permissible limits set by environmental protection agency which ensures that the treated water is free from all main toxicants and is suitable for potable purposes. The low content of phosphate in effluent water further indicates that phosphate is the main competitor of fluoride ion in adsorption process. No leaching of the metal ions from the adsorbent was found as no traces of metal ions of the adsorbent was reported in elute sample making it a robust, sustainable and reusable mixed oxide nanoadsorbent for fluoride removal. The performance of developed adsorbent was related to 80% fluoride removal at a pH value of 8.4 in real water samples analyses.

Conclusions

The nanoadsorbent showed that most favorable pH range for fluoride uptake is from 5.0–7.0 with an adsorbent dose of 0.4 g L⁻¹ of the fluoride solution having 10 mg L⁻¹ initial fluoride ions concentration. It gave the highest adsorption efficiency of 98.7%. Kinetic data fitted well into pseudo-second-order kinetic model. The adsorption isotherm illustrated the Freundlich and D-R isotherm models equally well. A high adsorption capacity of 285.7 mg g⁻¹ was achieved using equilibrium fluoride concentration of 10 mg L⁻¹, adsorbent dose 0.4 g L⁻¹, contact time 30 min and at pH 7.0. Surface properties of the adsorbent were described using BET equation. The FESEM and EDS analyses supported the mechanism of adsorption process and formation of adsorbent with high purity. The FTIR analysis demonstrated the involvement of ion exchange mechanism for fluoride uptake. Thermodynamic investigation illustrated spontaneous nature of fluoride uptake with the increase of entropy of the system.

Acknowledgments

We are thankful to Professor Aditya Shastri Vice-Chancellor of Banasthali University, Rajasthan, for kindly extending the facilities of “Banasthali Centre of Education” for research in basic sciences sanctioned under CURIE programme of the Department of Science and Technology, New Delhi and Dr. Tokker Ahmad, Jamia Millia Islamia University, New Delhi for helping us in BET analysis.

References

1. M. Amini, K. Mueller, K. C. Abbaspour, T. Rosenberg, M. Afyuni, K. N. Møller, M. Sarr and C. A. Johnson, *Environ. Sci. Technol.*, 2008, **42**, 3662–3668.
2. B. M. Rahmani, A. H. Mahvi, S. Dobaradaran and S. S. Hosseini, *Int. J. Environ. Sci. Tech.*, 2009, **6**, 629–632.
3. S. J. Gaciri and T. C. Davies, *J. Hydrol.*, 1993, **143**, 395–412.
4. W. Czarnowski, K. Wrzesniowska and J. Krechniak, *Sci. Total Environ.*, 1996, **191**, 177–184.
5. N. Azbar and A. Turkman, *Water Sci. Technol.*, 2000, **42**, 403–407.
6. M. Agarwal, K. Rai, R. Shrivastav and S. Dass, *J. Cleaner Prod.*, 2003, **11**, 439–444.
7. N. Mameri, A. R. Yeddou, H. Lounici, D. Belhocine, H. Grib and B. Bariou, *Water Res.*, 1998, **32**, 1604–1612.
8. Y. Shan and H. Guo, *Chem. Eng. J.*, 2013, **223**, 183–191.
9. H. Mjengera and G. Mkongo, *Phys. Chem. Earth*, 2003, **28**, 1097–1104.
10. F. Diaz-Barriga, A. Navarro-Quezada, M. Grijalva, M. Grimaldo, J. P. Loyola-Rodriguez and M. D. Ortiz, *Fluoride*, 1997, **30**, 233–239.
11. E. Kruse and J. Ainchil, *Argentina Environ. Geol.*, 2003, **44**, 86–89.
12. WRC, Distribution of fluoride-rich groundwater in Eastern and Mogwase region of Northern and North-west province, WRC Report No. 526/1/01 1.1–9.85 Pretoria, 2001.
13. I. Abe, S. Iwasaki, T. Tokimoto, N. Kawasaki, T. Nakamura and S. Tanada, *J. Colloid Interface Sci.*, 2004, **275**, 35–39.
14. D. Banks, C. Reimann, O. Røyset, H. Skarphagen and O. M. Sæther, *Appl. Geochem.*, 1995, **10**, 1–16.
15. A. Goswami and M. K. Purkait, *Sep. Sci. Technol.*, 2011, **46**, 1797–1807.
16. W. B. Apambire, D. R. Boyle and F. A. Michel, *Environ. Geochem.*, 1997, **33**, 13–24.
17. N. B. Reddy and K. S. S. Prasad, *Indian J. Environ. Health*, 2003, **45**, 285–288.

18. E. J. Reardon and Y. Wang, *Environ. Sci. Technol.*, 2000, **34**, 3247–3253.
19. F. Shen, X. Chen, P. Gao and G. Chen, *Chem. Eng. Sci.*, 2003, **58**, 987–993.
20. G. de la Puente, J. J. Pis, J. A. Menendez and P. Grange, *J. Anal. Appl. Pyrolysis*, 1997, **43**, 125–138.
21. S. Ayoob and A. K. Gupta, *Crit. Rev. Environ. Sci. Technol.*, 2006, **36**, 433–487.
22. Fluoride in Drinking Water: A Scientific Review of EPA's Standards. Washington, DC: The National Academies Press, 2006.
23. C. L. Bell, F. W. Brownell, D. R. Case, K. A. Ewing, J. O. King, S. W. Landfair, D. K. McCall III, M. L. Miller, K. J. Nardi, A. P. Olney, T. Richichi, J. M. Scagnelli, J. W. Spensley, D. M. Steinway, R. R. von Oppenfeld, *Environmental Law Handbook*, 22 Edition, Bernan Press, 2013.
24. M. Mahramanlioglu, I. Kizilcikli and I. O. Bicer, *J. Fluorine Chem.*, 2002, **115**, 41–47.
25. N. J. Chinoy, *Indian J. Environ. Toxicol.*, 1991, **1**, 17–32.
26. P. T. C. Harrison, *J. Fluorine Chem.*, 2005, **126**, 1448–1456.
27. X. Fan, D. J. Parker and M. D. Smith, *Water Res.*, 2003, **37**, 4929–4937.
28. Y. Zhou, C. Yu and Y. Shan, *Sep. Purif. Technol.*, 2004, **36**, 89–94.
29. M. Islam and R. K. Patel, *Chem. Eng. J.*, 2011, **169**, 68–77.
30. K. Banerjee, G. L. Amy, M. Prevost, S. Nour, M. Jekel, P. M. Gallagher and C. D. Blumenschein, *Water Res.*, 2008, **42**, 3371–3378.
31. Q. Guo and J. Tian, *Chem. Eng. J.*, 2013, **231**, 121–131.
32. A. M. Raichur and M. J. Basu, *Sep. Purif. Technol.*, 2001, **24**, 121–127.
33. A. Tor, N. Danaoglu, G. Arslan and Y. Cengeloglu, *J. Hazard. Mater.*, 2009, **164**, 271–278.
34. A. Tor, *Desalination*, 2006, **201**, 267–276.
35. G. Alagumuthu and M. Rajan, *Chem. Eng. J.*, 2010, **158**, 451–457.
36. G. Alagumuthu and M. Rajan, *Hem. Ind.*, 2010, **64**, 295–304.
37. A. Tor, *J. Hazard. Mater.*, 2007, **141**, 814–818.
38. K. M. Papat, P. S. Anand and B. D. Dasare, *React. Polym.*, 1994, **23**, 23–32.
39. F. Luo and K. Inoue, *Solvent Extr. Ion Exch.*, 2004, **22**, 305–322.
40. I. B. Solangi, S. Memon and M. I. Bhangar, *J. Hazard. Mater.*, 2009, **171**, 815–819.
41. S. Meenakshi and N. Viswanathan, *J. Colloid Interface Sci.*, 2007, **308**, 438–450.
42. N. Viswanathan and S. Meenakshi, *J. Hazard. Mater.*, 2009, **162**, 920–930.

43. R. Malaisamy, A. Talla–Nwafo and K. L. Jones, *Sep. Purif. Technol.*, 2011, **77**, 367–374.
44. S. Chakraborty, M. Roy and P. Pal, *Desalination*, 2013, **313**, 115–124.
45. E. Ergun, A. Tor, Y. Cengeloglu and I. Kocak, *Sep. Purif. Technol.*, 2008, **64**, 147–153.
46. M. M. Emamjomeh, M. Sivakumar and A. S. Varyani, *Desalination*, 2011, **275**, 102–106.
47. U. T. Una, A. S. Kopalal and U. B. Ogutveren, *Chem. Eng. J.*, 2013, **223**, 110–115.
48. R. Simons, *Desalination*, 1993, **89**, 325–341.
49. P. Sehn, *Desalination*, 2008, **223**, 73–84.
50. S. K. Adhikary, U. K. Tipnis, W. P. Harkare and K. P. Govindan, *Desalination*, 1989, **71**, 301–312.
51. B. Kemer, D. Ozdes, A. Gundogdu, V. N. Bulut, C. Duran and M. Soylak, *J. Hazard. Mater.*, 2009, **168**, 888–894.
52. M. Mohapatra, S. Anand, B. K. Mishra, D. E. Giles and P. Singh, *J. Environ. Manage.*, 2009, **91**, 67–77.
53. P. Miretzky and A. F. Cirelli, *J. Fluorine Chem.*, 2011, **132**, 231–240.
54. Y. Tian, M. Wu, R. Liu, D. Wang, X. Lin, W. Liu, L. Ma, Y. Li and Y. Huang, *J. Hazard. Mater.*, 2011, **185**, 93–100.
55. M. Karthikeyan, K. K. S. Kumar and K. P. Elango, *Desalination*, 2011, **267**, 49–56.
56. A. Bhatnagar, E. Kumar and M. Sillanpää, *Chem. Eng. J.*, 2011, **171**, 811–840.
57. J. L. Davila–Rodriguez, V. A. Escobar–Barrios, K. Shirai and J. R. Rangel–Mendez, *J. Fluorine Chem.*, 2009, **130**, 718–726.
58. D. Thakre, S. Jagtap, N. Sakhare, N. Labhsetwar, S. Meshram and S. Rayalu, *Chem. Eng. J.*, 2010, **158**, 315–324.
59. S. M. Prabhu and S. Meenakshi, *Journal of Water Process Engineering*, 2014, **2**, 96–104.
60. B. Zhao, Y. Zhang, X. Dou, X. Wu and M. Yang, *Chem. Eng. J.*, 2012, **185–186**, 211–218.
61. L. Chen, B. Y. He, S. He, T. J. Wang, C. L. Su, and Y. Jin, *Powder Technol.*, 2012, **227**, 3–8.
62. J. Kim and B. V. der Bruggen, *Environ. Pollut.*, 2010, **158**, 2335–2349.
63. W. X. Gong, J. H. Qu, R. P. Liu and H. C. Lan, *Chem. Eng. J.*, 2012, **189–190**, 126–133.

64. L. Borah and N. C. Dey, *Indian J. Chem. Technol.*, 2009, **16**, 361–363.
65. G. Moges, F. Zewge and M. Socher, *J. African Earth Sci.*, 1996, **22**, 479–482.
66. P. P. Coetzee, L. L. Coetzee, R. Puka and S. Mubenga, *Water SA*, 2003, **29**, 331–338.
67. G. Karthikeyan, A. Pius and G. Alagumuthu, *Indian J. Chem. Technol.*, 2005, **12**, 263–272.
68. A. Teutli–Sequeira, V. Martí'nez–Miranda, M. Solache–Ri'os and I. Linares–Herna'ndez, *J. Fluorine Chem.*, 2013, **148**, 6–13.
69. N. Hamdi and E. Srasra, *Desalination*, 2007, **206**, 238–244.
70. M. Sarkar, A. Banerjee, P. P. Pramanick and A. R. Sarkar, *J. Colloid Interface Sci.*, 2006, **302**, 432–441.
71. J. Boken, S. Thatai, P. Khurana, S. Prasad and D. Kumar, *Talanta*, 2014, **132**, 274–284.
72. V. Tomar, S. Prasad and D. Kumar, *Microchem. J.*, 2013, **111**, 116–124.
73. S. Thatai, P. Khurana, S. Prasad and D. Kumar, *Microchem. J.*, 2014, **113**, 77–82.
74. V. Tomar and D. Kumar, *Chem. Cent. J.*, 2013, **7**, 51.
75. M. Kruk and M. Jaroniec, *Chem. Mater.*, 2001, **13**, 3169–3183.
76. K. S. W. Sing, D. H. Everett, R. A. W. Haul, L. Moscou, R. A. Pierotti, J. Rouquerol and T. Siemieniewska, *Pure Appl. Chem.*, 1985, **57**, 603–619.
77. M. Kruk and M. Jaroniec, *Chem. Mater.*, 2000, **12**, 222–230.
78. T. Ahmad, S. Khatoon, S. E. Lofland and G. S. Thakur, *Mater. Sci. Semicond. Process.*, 2014, **17**, 207–215.
79. G. E. J. Poinern, M. K. Ghosh, Y. J. Ng, T. B. Issa, S. Anand and P. Singh, *J. Hazard. Mater.*, 2011, **185**, 29–37.
80. A. Gil, S. A. Korili and G. Y. Cherkashinin, *J. Colloid Interface Sci.*, 2003, **262**, 603–2607.
81. J. D. Russell, *Clay Miner.*, 1979, **14**, 109–114.
82. M. G. Sujana and S. Mohanty, *Int. J. Eng. Sci.*, 2010, **2**, 1–12.
83. C. Gao, X. Y. Yu, T. Luo, Y. Jia, B. Sun, J. H. Liu and X. J. Huang, *J. Mater. Chem. A*, 2014, **2**, 2119–2128.
84. T. F. Lv, W. Ma, G. Xin, R. Wang, J. Xu, D. M. Liu, F. J. Liu and D. C. Pan, *J. Hazard. Mater.*, 2012, **237**, 121–132.
85. X. Wang and L. Andrews, *J. Phys. Chem. A*, 2006, **110**, 10035–10045.
86. S. Jagtap, M. K. N. Yenkie, N. Labhsetwar and S. Rayalu, *Micropor. Mesopor. Mater.*, 2011, **142**, 454–463.

87. H. M. F. Freundlich, *Z. Phys. Chem.*, 1906, **57A**, 385–470.
88. I. Langmuir, *J. Am. Chem. Soc.*, 1916, **38**, 2221–2295.
89. G. Zhang, Z. He and W. Xu, *Chem. Eng. J.*, 2012, **183**, 315–324.
90. G. Patel, U. Pal and S. Menon, *Separ. Sci. and Technol.*, 2009, **44**, 2806–2826.
91. S. K. Swain, T. Patnaik and R. K. Dey, *Desalin. Water Treat.*, 2013, **51**, 4368–4378.
92. V. Tomar, S. Prasad and D. Kumar, *Microchem. J.*, 2014, **112**, 97–103.
93. Y. Ku and H. M. Chiou, *Water Air. Soil Pollut.*, 2002, **133**, 349–360.
94. K. Vijayaraghavan, T. V. N. Padmesh, K. Palanivelu and M. Velan, *J. Hazard. Mater. B*, 2006, **133**, 304–308.
95. C. F. Chang, C. Y. Chang and T. L. Hsu, *Desalination*, 2011, **279**, 375–382.
96. N. Viswanathan, C. S. Sundaram and S. Meenakshi, *J. Hazard. Mater.*, 2009, **161**, 423–430.
97. S. K. Swain, T. Patnaik, V. K. Singh, U. Jha, R. K. Patel and R. K. Dey, *Chem. Eng. J.*, 2011, **171**, 1218–1226.
98. S. K. Swain, S. Mishra, T. Patnaik, R. K. Patel, U. Jha and R. K. Dey, *Chem. Eng. J.*, 2012, **184**, 72–81.
99. S. Y. Lagergren, *Kungliga Svenska Vetenskapsakad Handl.*, 1898, **24**, 1–39.
100. C. S. Sundaram, N. Viswanathan and S. Meenakshi, *Bioresour. Technol.*, 2008, **99**, 8226–8230.
101. Y. S. Ho and G. McKay, *Process Biochem.*, 1999, **34**, 451–465.
102. D. Robati, *J. Nanostructure Chem.*, 2013, **3**, 55.
103. J. Zhou, Y. Cheng, J. Yu and G. Liu, *J. Mater. Chem.*, 2011, **21**, 19353–19361.
104. M. H. Jnr and A. Spiff, *Electron. J. Biotechnol.*, 2005, **8**, 162–169.
105. E. Eren, *J. Hazard. Mater.*, 2008, **159**, 235–244.
106. N. Viswanathan, S. M. Prabhu and S. Meenakshi, *J. Fluorine Chem.*, 2013, **153**, 143–150.
107. W. Wei, X. Wang, Y. Wang, M. Xu, J. Cui and Z. Wei, *Desalin. Water Treat.*, 2013, 1–11.
108. Y. Vijaya, M. V. Subbaiah, A. S. Reddy and A. Krishnaiah, *Desalin. Water Treat.*, 2010, **20**, 272–280.
109. M. Mourabet, A. E. Rhilassi, H. E. Boujaady, M. B. Ziatni, R. E. Hamri and A. Taitai, *Appl. Surf. Sci.*, 2012, **258**, 4402–4410.
110. A. A. M. Daifullah, S. M. Yakout and S. A. Elreefy, *J. Hazard. Mater.*, 2007, **147**, 633–643.

111. N. Chen, Z. Zhang, C. Feng, M. Li, R. Chen and N. Sugiura, *Desalination*, 2011, **268**, 76–82.
112. S. Mandal and S. Mayadevi, *J. Hazard. Mater.*, 2009, **167**, 873–878.
113. S. Gao, R. Sun, Z. Wei, H. Zhao, H. Li and F. Hua, *J. Fluorine Chem.*, 2009, **130**, 550–556.
114. N. Thakur, S. A. Kumar, D. N. Wagh, S. Das, A. K. Pandey, S. D. Kumara and A. V. R. Reddy, *J. Hazard. Mater.*, 2012, **201–202**, 193–201.
115. Y. Wang, N. Chen, W. Wei, J. Cui and Z. Wei, *Desalination*, 2011, **276**, 161–168.
116. M. G. Sujana and S. Anand, *Appl. Surf. Sci.*, 2010, **256**, 6956–6962.
117. M. Srimurali, A. Pragathi and J. Karthikeyan, *Environ. Pollut.*, 1998, **99**, 285–289.
118. S. V. Ramanaiah, S. V. Mohan and P. N. Sarma, *Ecol. Eng.*, 2007, **31**, 47–56.
119. Q. Guo and E. J. Reardon, *Appl. Clay Sci.*, 2012, **56**, 7–15.
120. M. Vithanage, L. Jayarathna, A. U. Rajapaksha, C. B. Dissanayake, M. S. Bootharaju and T. Pradeep, *Colloids and Surfaces A: Physicochem. Eng. Aspects*, 2012, **398**, 69–75.
121. S. Chakrabarty and H. P. Sarma, *Int. J. Chem. Tech. Res.*, 2012, **4**, 511–516.
122. A. K. Yadav, R. Abbassi, A. Gupta and M. Dadashzadeh, *Ecol. Eng.*, 2013, **52**, 211–218.
123. Y. Zhao, X. Li, L. Liu and F. Chen, *Carbohydr. Polym.*, 2008, **72**, 144–150.
124. K. Biswas, D. Bandhoyapadhyay and U. C. Ghosh, *J. Environ. Science & Engg.*, 2008, **50**, 153–162.
125. K. Biswas, K. Gupta, A. Goswami and U. C. Ghosh, *Desalination*, 2010, **255**, 44–51.
126. H. Liu, S. Denga, Z. Li, G. Yua and J. Huang, *J. Hazard. Mater.*, 2010, **179**, 424–430.
127. L. X. Li, D. Xu, X. Q. Li, W. C. Liu and Y. Jia, *New J. Chem.*, 2014, **38**, 5445–5452.
128. F. Adeno, E. Mulugeta, F. Zewge and Y. Chebude, *Bull. Chem. Soc. Ethiop.*, 2014, **28**, 215–227.
129. A. Mahapatra, B. G. Mishra and G. Hota, *Ind. Eng. Chem. Res.*, 2013, **52**, 1554–1561.
130. N. Thakur S. A. Kumar, H. Parab, A. K. Pandey, P. Bhatt, S. D. Kumar and A. V. R. Reddy, *RSC Adv.*, 2014, **4**, 10350–10357.
131. X. Zhao, J. Wang, F. Wu, T. Wang, Y. Cai, Y. Shi and G. Jiang, *J. Hazard. Mater.*, 2010, **173**, 102–109.
132. Y. Huo, W. Ding, X. Huang, J. Xu and M. Zhao, *Chin. J. Chem. Eng.*, 2011, **19**, 365–370.

133. S. Deng, H. Liu, W. Zhou, J. Huang and G. Yu, *J. Hazard. Mater.*, 2011, **186**, 1360–1366.
134. J. Liu, L. Wan, L. Zhang and Q. Zhou, *J. Colloid Interface Sci.*, 2011, **364**, 490–496.
135. J. Liu, Q. Zhou, J. Chen, L. Zhang and N. Chang, *Chem. Eng. J.*, 2013, **215–216**, 859–867.
136. L. Zhang, Q. Zhou, J. Liu, N. Chang, L. Wan and J. Chen, *Chem. Eng. J.*, 2012, **185–186**, 160–167.
137. E. T. Kamga, E. Ngameni and A. Darchen, *J. Colloid Interf. Sci.*, 2010, **346**, 494–499.
138. X. Dou, Y. Zhang, H. Wang, T. Wang and Y. Wang, *Water Res.*, 2011, **45**, 3571–3578.
139. T. Li, Z. Zhu, D. Wang, C. Yao and H. Tang, *Powder Technol.*, 2006, **168**, 104–110.
140. R. L. Ramos, J. O. Turrubiartes and M. A. S. Castillo, *Carbon*, 1999, **37**, 609.
141. Y. H. Li, S. Wang, X. Zhang, J. Wei, C. Xu, Z. Luan and D. Wu, *Mater. Res. Bull.*, 2003, **38**, 469–476.